Sedimentation and rheological behavior of reactive and non-reactive magnesium hydroxide pulps for industrial spray dryer processing

E. C. Campos[1], D. H. S. Chaves[1], C. M. F. Santos[1], S. D. F. Rocha[2], V. S. Birchal[1]*

[1]*Universidade Federal de Minas Gerais, Graduate Program in Chemical Engineering, 31270-901, Av. Pres. Antônio Carlos 6627, Belo Horizonte, MG, Brazil*

[2]*Universidade Federal de Minas Gerais, Mining Engineering Department, 31270-901, Belo Horizonte, MG, Brazil*

Abstract

Two different reactive concentrated magnesium hydroxide (HM) pulps, produced in a lab reactor mill, and a synthetic and non-reactive HM-pulp, for comparative analyses, have been prepared and studied. Sodium polyacrylate was selected as a dispersant for improving the HM pulp fluidity, with concentrations varying from 0.42% to 2.0% on a dry basis. The two reactive pulps differed from each other mainly by the impurity level and for both, a residual MgO amount was detected, implying that the hydration reaction could proceed. Results (with and without dispersant) confirmed the formation of particle clusters as HM concentration rose until a critical value, above which the pulp behaved as a solid. Reactive HM-pulps with high impurities may represent a limiting factor in the drying operation. Among all HM-pulps studied, the purest reactive pulp with 1% dispersant presented the best flow behavior making this reactive pulp the most suitable to be tested in a pilot spray dryer.

Keywords: physical-chemical characterization, rheology, sedimentation, stability, structural particle arrangements.

INTRODUCTION

In the last few decades, the interest in magnesium hydroxide (HM), $Mg(OH)_2$, has grown due to its use in several industrial processes, such as: alkali agent, adsorbent of heavy metals and organic contaminants in wastewater, and effluent treatments [1, 2]; fire retardant in polymers and epoxy resins [3, 4]; silica removal and desulfurization of environments [2, 5]; bleach and preservative in the papermaking process [6]; fertilizer in the agricultural sector [7]; stabilizer for controlled release of biologically active proteins [8]; and precursor in the production of other magnesium compounds [9]. Caustic magnesia hydration is one of the most known and advantageous routes to obtain HM, especially in countries with natural magnesite ore reserves, such as China, Turkey, Russia, and Brazil, which are responsible for more than half of the world's magnesite mine production [10]. The reaction mechanism comprises three main steps: the magnesium oxide dissolution, the solution supersaturation by magnesium and hydroxyl ions, and the hydroxide precipitation. This latter step represents a barrier in the process yield because HM formed is just deposited on the MgO particle surface, slowing and/or ending the reaction [11, 12]. Therefore, improvements are demanded in HM production, making processes more profitable and feasible to generate particles with the sizes and morphology required by the actual market demand.

Generally, mineral pulps behave as viscoelastic materials with predominant viscous behavior but with solid-like characteristics [13]. Concentrated HM pulps with solid concentration $C_s \geq 35$ wt% are difficult to handle, pump, and process because of their high apparent viscosity (η>5-10 Pa.s at low shear rates) and due to the tendency to stick together in a cake form, making impossible its reconstitution in water [14, 15]. Furthermore, if these pulps are not continuously agitated, particles may aggregate by interconnecting themselves into a lattice structure and due to water expulsion, resulting in irreversible networks that behave as a rigid solid [1, 16, 17]. This problem affects the transportation, processing, and storage of concentrated HM pulps, so, it encourages new advances in producing HM powder with specific properties. A new route for HM production is proposed using an equipment that performs simultaneously the MgO hydration reaction and the particle comminution [18]. The spray dryer is suggested to replace the commonly used rotary dryer to be able to form HM powder with predefined characteristics. Using a lab reactor mill and caustic magnesia with 98.2% of MgO, the technical feasibility of performing the MgO hydration reaction and the particle comminution simultaneously has been confirmed reaching conversions of MgO to HM up to 5% higher than one obtained in a conventional caustic magnesia hydration route (CSTR) under the same operation conditions [18]. The feasibility of using the spray dryer for producing powder from these HM pulps requires knowledge of their sedimentation behavior, their rheology as well as their particle size distribution. There are no studies yet on sedimentation and the rheological behavior of reactive HM

**diegohschaves@outlook.com*
https://orcid.org/0000-0002-4611-9256

pulps. Reactive pulps prepared from different sources of caustic magnesia may behave differently during continuous operation due to different purity contents.

This work aims to analyze the characteristics and stability of reactive HM pulps produced in a reactor mill equipment for evaluating the feasibility of drying them in a spray dryer. Therefore, two different reactive and concentrated HM-pulps produced in a lab reactor mill were characterized concerning the chemical composition, physical properties (density, particle size, and structure), sedimentation stability, and rheological behavior. For comparison of results, synthetic and non-reactive pulps prepared by a standard commercial HM powder were also characterized using the same methodology. As these pulps have high solid concentrations, problems with their pumping and atomization should be minimized to allow drying operation. Thus, the addition of a dispersant to these pulps for improving their fluidity was also analyzed.

MATERIALS AND METHODS

Preparation of magnesium hydroxide pulps: the HM pulps have been produced in a reactor mill under optimum operating conditions [18]: feed: caustic magnesia suspension varying from 25 to 30 wt% and 0.2 mol/L acetic acid (Labsynth, Brazil); initial temperature=25 °C; operating time=5 h. The reactor mill equipment had an internal volume corresponding to 2.0 L with a diameter of 0.12 m and a height of 0.18 m. Caustic magnesia came from two different Brazilian mineral sources: magnesia A with 91% of MgO and magnesia B with 99% of MgO. HM pulps left the reactor mill in the pH range from 11 to 12 (11.8 on average) and remained at this range due to the buffer effect of HM suspensions [18]. HM-A and HM-B pulps were produced for each test performed since they were reactive and hence could not be stored and/or processed for more than 3 h (stable time scale) at 25 °C. Samples were taken from these pulps to determine: i) solid concentration, C_s ($=m_s/m_{susp}$), by measuring the sample mass (m_{susp}) and the solids mass (m_s), which was made after washing the sample with acetone R.G. (Labsynth, Brazil) and drying it in an oven (Med-Clave, LTE Scient., UK) at 120 °C for 2 h; ii) magnesium hydroxide concentration in dry basis, $X_{HM}=m_{HM}/m_s$ (HM mass/solid mass), by calculating m_{HM} as a sum of the HM mass generated by the MgO hydration reaction plus one already presented in the precursor sample [18]. Mass measurements were made in a high-precision analytical balance (AY220, Shimadzu, USA) in triplicate. Synthetic HM pulps (HM-R) were prepared from a commercial HM powder, analytical standard with 97% of purity and $9.5 \leq pH \leq 10.5$ (Labsynth, Brazil). To obtain the desired HM-R solid concentration, HM-R powder was added to distilled water inside a glass beaker (Prolab, Brazil) with a mechanical stirrer (713D, Fisatom, Brazil) under a constant agitation of 650 rpm. The NaPA dispersant (KemEcal 211, Kemira Chem., Brazil) had a low molar mass and it came as a light amber aqueous solution with 40% of solid concentration (in mass), pH of 7 to 8, density and viscosity at 25 °C equal to 1300 kg/m^3 and 0.045 to 0.070 Pa.s, respectively. This solution was added to HM pulps under a constant agitation of 650 rpm. Preliminary tests performed in a digital rotary viscometer (LVDV-I Prime, Brookfield, USA) defined the working range of the dispersant concentration, which was expressed in dry basis, $X_{disp}=m_{disp}/m_s$. The selected X_{disp} range used in experiments was: 0.42% to 2% for HM-R pulps and 1% to 2% for HM-A and HM-B pulps. This range was in accordance with the recommended literature: $m_{NaPA}/m_s \geq 0.6\%$ (corresponding to $X_{disp} \geq 1.5\%$ for KemEcal 211 solution) [1] and $0.30\% \leq X_{disp} \leq 3.50\%$ [19]. $X_{disp}=3\%$ was also used, when necessary, to complement data.

Solids characterization: the HM pulp characterization included: i) identification of mineral crystalline phases by the X-ray diffraction using a diffractometer (PW 1710, Philips-PANalytical, Netherlands) equipped with copper anode (characteristic Kα radiation); ii) measurements, in triplicate, of density at 25 °C by the pycnometric method, using the high precision analytical balance and a calibrated 10 mL glass pycnometer (Prolab, Brazil); iii) determination of particle size distribution by the laser diffraction equipment (Helos12LA, Sympatec, Germany) using the following procedure: filtering (Labsynth, Brazil; filter blue/purple dot) and washing the particle samples with acetone R.G. to avoid further MgO hydration reaction; drying them in an oven (Med-Clave, LTE Scient., UK) at 120 °C for 2 h; dispersion of 1 g of particle sample in a sodium hexametaphosphate solution (Labsynth, Brazil) and homogenization of the dispersion in an ultrasonic system (Vibra-cell, Sonics, USA) with 2.5 s pulsation to minimize particle agglomeration; and carrying out the test in the laser diffraction equipment.

Sedimentation experiments: these experiments were performed by a traditional batch method. After preparing the HM pulp (with or without dispersant), it was well homogenized with the mechanical stirrer (713D, Fisatom, Brazil) at 650 rpm, and a 250 mL aliquot was transferred to a glass graduated cylinder (Prolab, Brazil). This aliquot was then stirred with a glass rod (Prolab, Brazil) to prevent the adherence of particles to the cylinder wall. Since HM pulps were concentrated, Stokes law could not be applied to calculate the particle settling velocity, v_{sed} [20]. This velocity is straightly related to the type of interaction forces between particles/aggregates and can be estimated by the numerical differentiation, using the central difference formula of two points or four points [21].

Rheological behavior experiments: experiments for determining the rheological behavior of HM pulps were performed in a properly calibrated rotary viscometer (LVDV-I Prime, Brookfield, USA) with the R13 adapter for processing small fluid samples (8 mL) and the SC04-18 coaxial cylindrical rotor (range: 0.003 to 10 Pa.s). The experimental procedure for these tests was adapted from the ASTM D2196-05 standard and from the viscometer-specific manual for sticky substances. Two data sets were produced to analyze the rheological behavior of HM pulps at three different temperatures: 27, 35, and 50 °C (±2 °C). One set

comprised three cycles of runs that generated data to obtain curves of shear stress, τ, as a function of the shear rate, $\dot{\gamma}$, for decreasing and increasing $\dot{\gamma}$ continuously. In this data set, the apparent viscosity, η, and τ were recorded at $\dot{\gamma}$ = 132, 66, 23.4, and 13.2 s^{-1}. The first cycle involved measurements in a descending shear-rate ramp while the second one, which followed immediately the first, was in an ascending shear-rate ramp. The third cycle involved measurements in a descending shear-rate ramp after resting the sample for a few seconds. The other data set included two runs that generated data to obtain curves of τ in the function of time, t, during 20 min at two distinct values of $\dot{\gamma}$ (132 and 60 s^{-1}). Measurements in both sets of experiments were made after the time required for stabilizing the viscosimeter reading (30 to 60 s). These data sets were replicated for each HM pulp used at each temperature, for determining the experimental error.

RESULTS AND DISCUSSION

Chemical characterization: X-ray diffractograms obtained for HM pulps are shown in Fig. 1. For the HM-R (Fig. 1a), brucite was the Mg carrier phase, identified in the characteristic peaks of 2θ (18°, 33°, 51°, 59°, 63°, 72°, 82°) using ICDD data. Other minority minerals were also detected as those containing Mg (chlorite, talc, magnesite, dolomite) and Ca (calcite). For HM-A (Fig. 1b) and HM-B (Fig. 1c), brucite was identified in the characteristic peaks of 2θ at 18°, 38°, 51°, 59°, and 63°, and 18°, 33°, 38°, 51°, 59°, 63°, 72°, and 82°, respectively. In HM-B, the mineral containing Ca was only calcite, while in HM-A dolomite was also detected. As expected, in HM-A and HM-B pulps, residual periclase was identified, indicating that MgO hydration reaction could proceed, slowly or fast, depending on the pulp conditions. There was no trace of periclase in the synthetic HM-R pulp. In addition to the minerals identified in Fig. 1, the presence of iron (Fe), manganese (Mn), and traces of titanium (Ti), copper (Cu), sulfur (S), phosphorus (P), and chlorine (Cl) were confirmed in HM-R. Traces of Fe and Mn were also confirmed in HM-A and HM-B pulps. By the quantitative and qualitative X-ray fluorescence analysis of the HM-R powder, the concentration of HM (calcined form=MgO) was in the range of 97%, corroborating the value supplied by the manufacturer.

Particle size analysis of solids in magnesium hydroxide pulps: the diameters $D_{15.9}$, D_{50}, and $D_{84.1}$ (particle/cluster size diameter for the cumulative distribution of 15.9%, 50%, and 84.1%, respectively) for the solid phase of HM-R, HM-A, and HM-B pulps with their particle size dispersion index, ID, defined by Eq. A are presented in Table I, which also summarizes C_s and X_{HM} values obtained for HM pulps analyzed. It was possible to verify that D_{50} for HM-R particles was up to 28% above D_{50} for HM-A30 and HM-B32 particles. However, this 28% was in the range of experimental error by considering the mean value of D_{50}=6.7±1.0 μm for HM-A (HM-A30 and HM-A34) and D_{50}=5.6±1.0 μm for HM-B

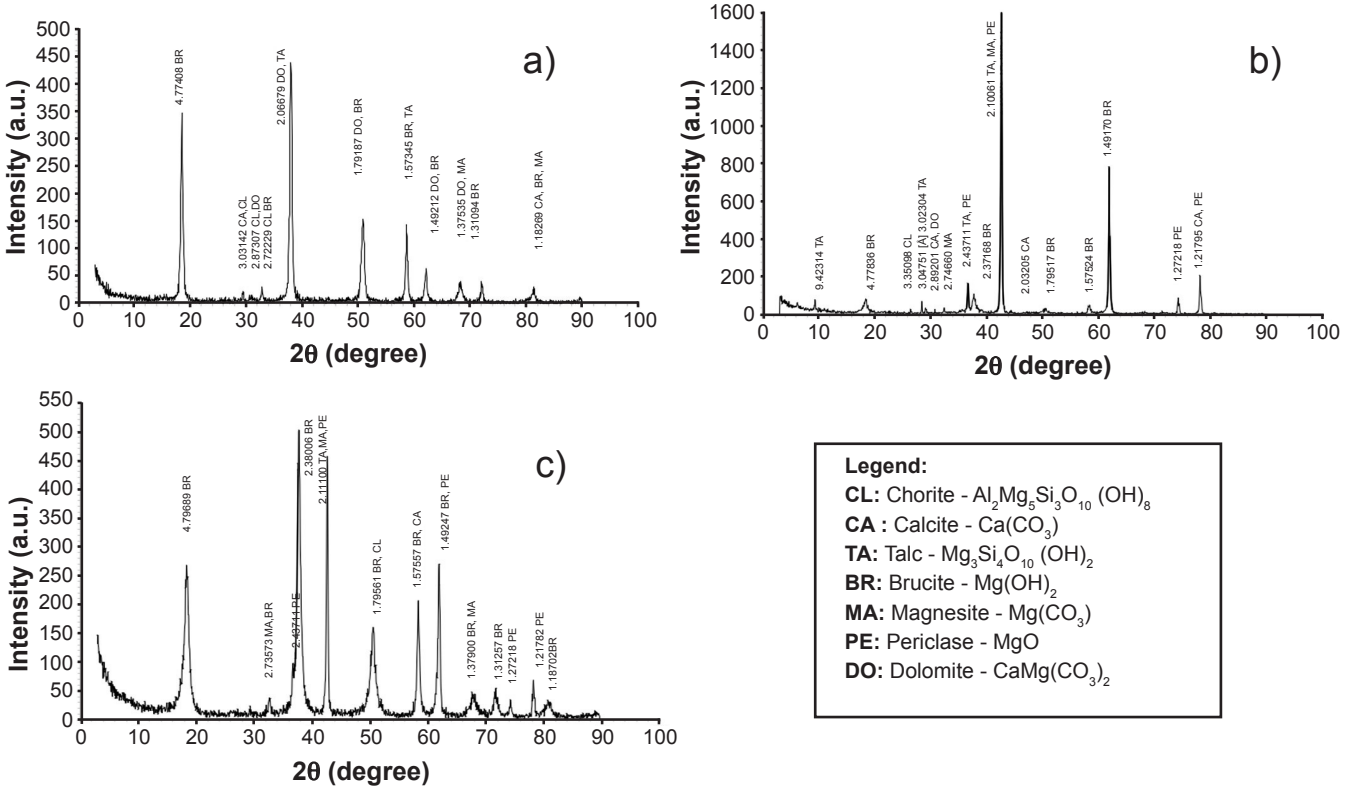

Figure 1: X-ray diffractograms with characteristic peaks of minerals present in: a) HM-R; b) HM-A; and c) HM-B pulps. The number above each diffraction peak is the interplanar distance in Å.

(HM-B32 and HM-B39). Although these three HM pulps presented a similar D_{50} particle size for the solid phase, their particle size dispersion index, ID, was different, indicating that HM-R particles presented the widest particle size dispersion. It is important to emphasize that HM particles were aggregates of primary particles as shown in Fig. 2.

$$ID = \frac{D_{84.1} - D_{15.9}}{2D_{50}} \quad (A)$$

As seen in Fig. 2, HM particles obtained in a CSTR (conventional caustic magnesia hydration route) were aggregated in different structures from those of HM particles produced in the reactor mill. This implied that the combination of the MgO hydration reaction with the particle comminution in a reactor mill affected the particle shape and surface area, and, consequently, the interconnections between particles. Since the HM-R powder was produced by another process route, its particle structural form should be quite different from that of HM-A and HM-B. HM production process is major responsible for first defining the structural arrangement and surface area of HM nanoparticles [22]. Consequently, the particle surface interactions with NaPA dispersant must differ between HM-R and HM-A or HM-B particles, explaining density ratio trends in Table II.

Magnesium hydroxide pulp density: results at 25 °C for the HM pulp density ratio, $\varrho_{susp,X}/\varrho_{susp,0}$ (with and without dispersant) are presented in Table II, together with experimental values of $\varrho_{susp,X}$ at X_{disp}. The overall error for ϱ_{susp} was ±3 kg/m^3 and the maximum error was ±11 kg/m^3. ϱ_{susp} increased with the increase in C_s moreover, ϱ_{susp} (C_s=30-35%) values for the three HM pulps were practically equal within an error lower than the maximum experimental one. This indicated the similarity in the mineralogical composition of the three pulps analyzed corroborating the pulp age stability during experiments (less than 3 h). Data from Table II demonstrated that the HM-R density ratio decreased with the dispersant addition (from 1.000 to 0.977 and then to 0.991). Although the HM-A density ratio tended to rise as X_{disp} increased, the values obtained remained in the same range of $\varrho_{susp,0}$ following the experimental error (±0.006). The HM-B ratio increased slightly with X_{disp}. Therefore, these three HM

Table I - Solid characterization of HM pulps analyzed.

HM pulp	C_s (%)	X_{HM} (%)*	$D_{15.9}$ (μm)	$D_{84.1}$ (μm)	D_{50} (μm)	ID
HM-A30	29.6	78.0	1.56	12.91	6.08	0.91±0.04
HM-A34	33.7	82.4	1.67	14.74	7.24	
HM-B32	32.4	90.3	1.61	12.41	5.91	0.89±0.04
HM-B39	38.6	90.8	1.58	10.74	5.25	
HM-R (powder)	N.A.	97.0				
HM-R20	20.0	97.0	2.63	15.60	6.74	0.96
HM-R30	30.0	97.0				
HM-R37	37.0	97.0				

*$C_s=m_s/m_{susp}$; $X_{HM}=m_{HM}/m_s$; *: % in dry basis; N.A.: not applicable.*

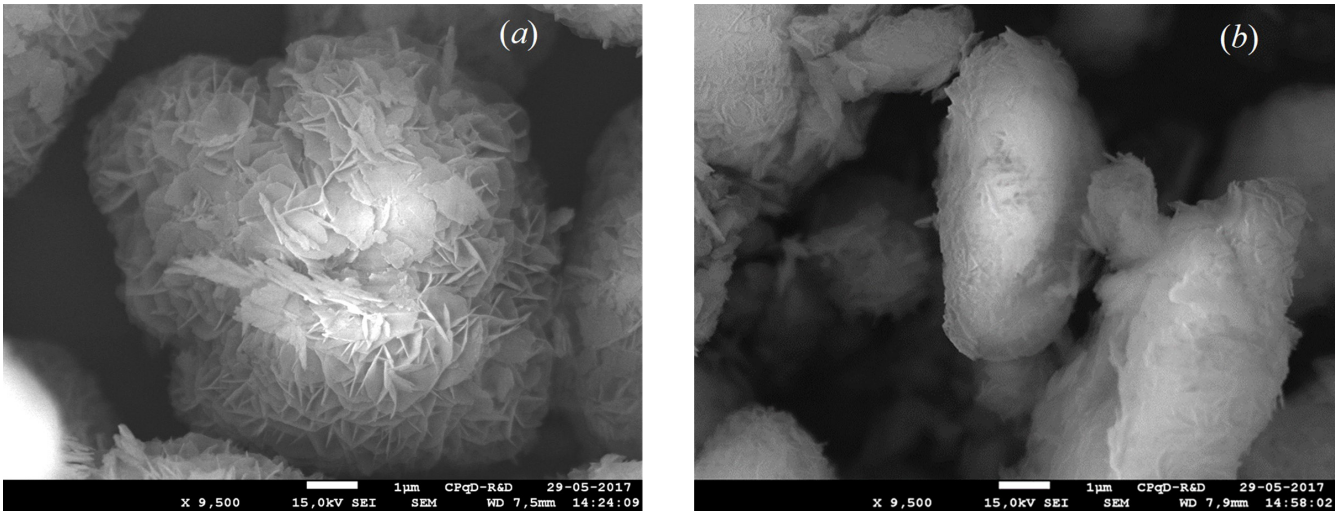

Figure 2: HM particles formed by the hydration of magnesia after 8 h of reaction in a CSTR (a) and reactor mill (b). Backscattered electron images obtained with a scanning electron microscope at 15 kV.

Table II - Densities of the HM pulps with dispersant at a preset dispersant concentration.

HM pulp with dispersant	X_{disp} (%)	$\varrho_{susp,X}$ (kg/m^3)	$\frac{\rho_{susp,X}}{\rho_{susp,o}}$
HM-R20-04	0.42	1122	0.987
HM-R20-08	0.84	1124	0.989
HM-R30-1	1.00	1176	0.977
HM-R30-2	2.00	1193	0.991
HM-A30-1	1.00	1208	1.002
HM-A30-2	2.00	1212	1.005
HM-B32-1	1.00	1219	1.010
HM-B32-2	2.00	1221	1.012

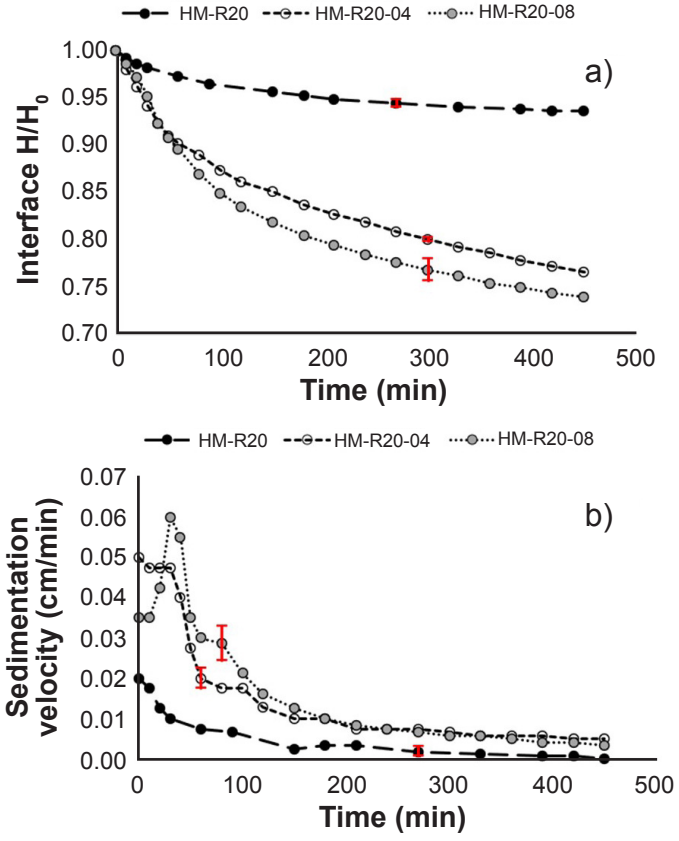

Figure 3: Sedimentation profile (a) and sedimentation velocity (b) curves as a function of time for HM-R20, HM-R20-04, and HM-R20-08 pulps.

pulps behaved differently when the dispersant was added as their values of $\varrho_{susp,X}/\varrho_{susp,0}$ differed from one another at the same C_s and X_{disp}. As analyzed in the particle size analysis of solids subsection, this difference in behavior may be related to particle morphology (size, shape, structural arrangement).

Sedimentation: the HM pulp sedimentation analysis focused on establishing parameters to well define the system stability, as well as, contributing to a better understanding of the bonds prevailing between particles and/or aggregates. In this analysis, sedimentation was expressed by its dimensionless parameter, H/H_0, experimental data points were interconnected by dotted lines without any statistical adjustment, and the experimental error based on replications was displayed, if necessary, in the respective curves obtained. The sedimentation velocity, v_{sed}, decreased exponentially with the increase in the solid concentration, C_s, in accordance with data and trends reported in the literature [21, 23]. For $C_s \geq 0.31$, v_{sed} tended to be negligible ($8x10^{-5}$ cm/s), meaning no sedimentation as a solid phase behavior [17]. Particle interconnections, especially those resulting in rigid three-dimensional networks, destabilize HM pulps, causing changes in their properties. Fig. 3 presents curves for HM-R20 pulps without dispersant, HM-R20-04, and HM-R20-08. As seen in Fig. 3b, the addition of dispersant increased v_{sed} at the initial sedimentation period (increased to 1.7 $v_{sed,HM-R20}$ for HM-R20-04 and to 2.5 $v_{sed,HM-R20}$ for HM-R20-08 both compared to HM-R20 at $X_{disp}=0$), because the particle mobility was enhanced due to enlarged space between particles promoted by the dispersant. However, preferential channels seemed to be formed for drainage of water expelled from the densest particle structure as the pulp was compressed at the container bottom (shown by peaks obtained).

Fig. 4 presents the v_{sed} vs. t curves for the HM-R30 (Fig. 4a) and for HM-R30-1 and HM-R30-2 (Fig. 4b) pulps. For HM-R30 pulp, the NaPA addition slowed slightly the H/H_0

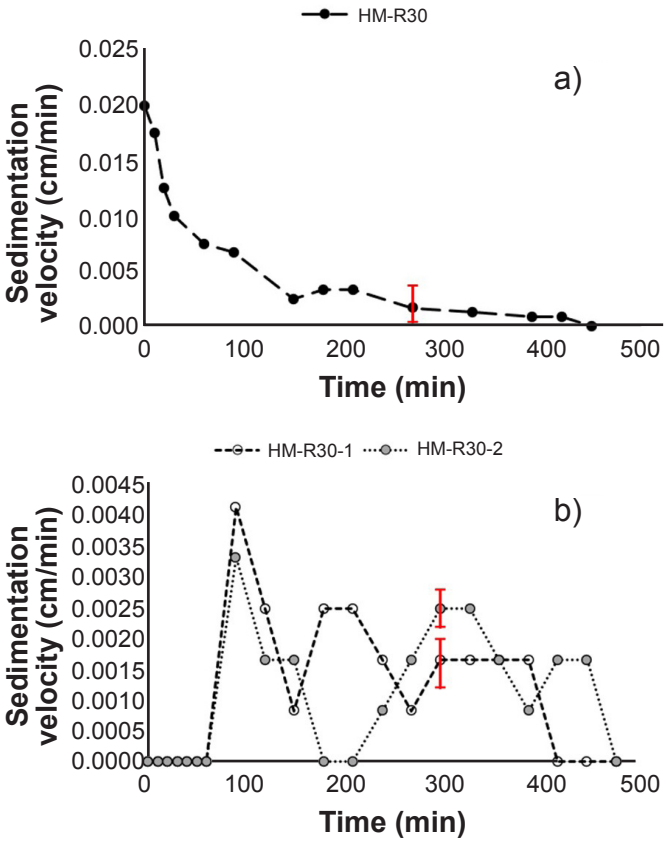

Figure 4: Sedimentation velocity as a function of time for HM-R30 (a), HM-R30-1 and HM-R30-2 (b) pulps.

decay at high dispersant concentrations (X_{disp}= 1% and 2%). These three curves provided additional information about particle interactions, showing noticeable peaks that resulted from preferential channels for flowing liquid (water). The formation of these channels induced an increase in v_{sed} followed by an abrupt decrease in v_{sed} due to water expulsion. This caused a highly compact pulp with clusters/aggregate consolidation in reticulated structures. As shown in Fig. 4b, an increase in disturbances in v_{sed} was observed at X_{disp}= 1% and 2%, denoting an increase in the preferential channel formation for water drainage. Due to the dispersant action, the weak particle interconnections were broken easily and rearranged continuously in new structures, resulting in the random formation and collapse of preferential channels. This caused great fluctuations in v_{sed} and restrained particle mobility. Sedimentation becomes significant on the time scale of the experiment since the radii of the aggregates/clusters become considerably large [21].

Fig. 5 shows data of sedimentation curves of HM-A30 without dispersant (Fig. 5a) and HM-A30-2 with X_{disp}=2% (Fig. 5b). The addition of dispersant resulted in: i) slowing down the interface decay with the drop of v_{sed}; ii) intensifying peaks and oscillations in the v_{sed} vs. t curve due to the preferential channel formation for water drainage from the compact structure in the container bottom. These trends were similar to those discussed for HM-R30. Although this work did not present HM-A30-1 data, its sedimentation had a transitional behavior between HM-A30 and HM-A30-2, showing that particle interactions were changing from flocculation to deflocculation. Data

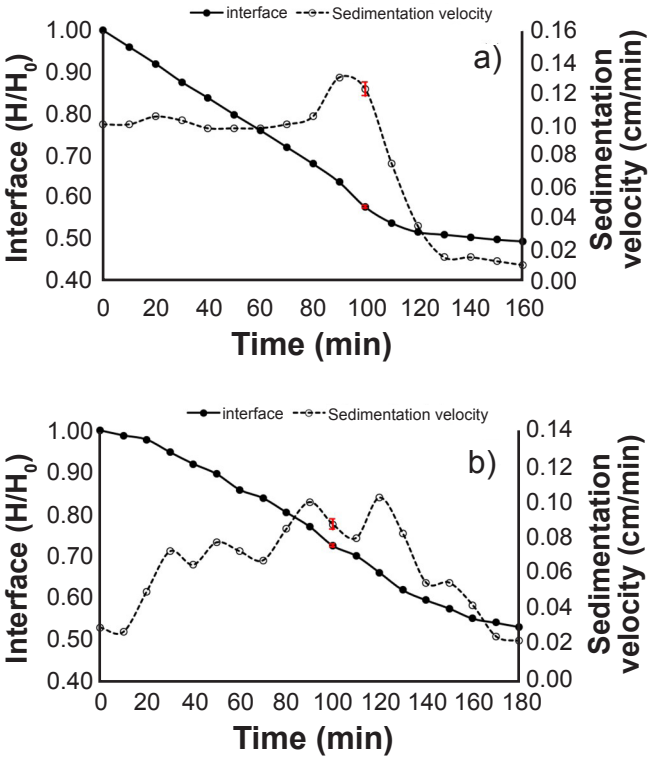

Figure 5: Sedimentation profile and velocity curves as a function of time for the pulps: a) HM-A30; and b) HM-A30-2

sedimentation for HM-A30-2 pulp showed the same trends of deflocculated suspension. The sedimentation curves for HM-A pulps produced in the reactor mill at C_s= 30% and 34%, exhibited a decrease of 50% in v_{sed} at the initial period as C_s increased. Similar to the HM-R pulp behavior, preferential channels also occurred in these HM-A pulps for drainage of water expelled from reticulated structures developed as the solid phase was compressed, but the v_{sed} oscillation was smoother (Fig. 5a). In contrast, in v_{sed} vs. t curves, a well-defined peak occurred just before the abrupt drop in v_{sed} with a significant deceleration of the solid phase compression. Visual observations confirmed the occurrence of small flocs (turbidity) in the first layer region of the HM-A pulp sample inside the cylinder. Such results suggested that the HM-A pulp sedimentation was characterized by particles that flocculated. HM-A pulps presented the lowest X_{HM} value, i.e., the highest impurity content, as well as, distinct particle morphology, which must have favored flocculation, in which attractive forces overlapped repulsive ones [24]. This corroborated the distinct behavior obtained for HM-A particle sedimentation and interconnections.

For HM-B32 pulp, the conventional sedimentation with a clarified-suspension interface formation was not detected even after 3 h of the experiment. Lumps and volcanoes were seen on the hard pulp surface and inside the dense pulp (with the removal of the pulp from the container after 3 h). The dispersant addition to this pulp, at X_{disp}= 1%, 2%, and even 3%, did not alter such behavior. From these sedimentation data, one can infer that there was a maximum C_s (of which value depended on X_{HM}) at which HM pulps behaved as a rigid solid, with the attraction forces between particles predominating over the repulsion ones. For HM-R pulps (X_{HM}=97%), $C_{s,max}$=0.31 as predicted from sedimentation curves. It was expected that $C_{s,max}$>0.34 for HM-A pulps ($X_{HM}\approx$ 81%) and 0.32<$C_{s,max}$<0.39 for HM-B pulp ($X_{HM}\approx$ 90%).

Rheological behavior

Reactive HM-B32 pulps: for HM-B32 pulp without dispersant, although data were limited by the device operation range, τ vs. t data showed that τ increased as the temperature was raised, as well as its value became more dependent on time (Fig. 6a). This behavior should be related with two distinct phenomena occurred in the HM-B32 pulp as the temperature rose: i) acceleration of MgO hydration reaction, which increased HM and reduced H_2O in the pulp, implying in an effective augment of C_s during the experiment; ii) formation of hydroclusters (particle aggregates in chain connections) that tends to enhance the pulp resistance to flow. Note that in concentrated suspensions with C_s close to $C_{s,max}$, a small change in C_s caused significant changes in the structural particle-aggregate [16]. In addition, hydroclusters should occur in concentrated suspensions because of the particle proximity and the hydrodynamic interparticle forces generated during shear flow [16, 21]. The shear flow with the hydrocluster occurrence may retard the rigid solid network formation seen in the sedimentation experiment of this HM-B32 pulp.

For HM-B32-1 pulp, τ decreased progressively with

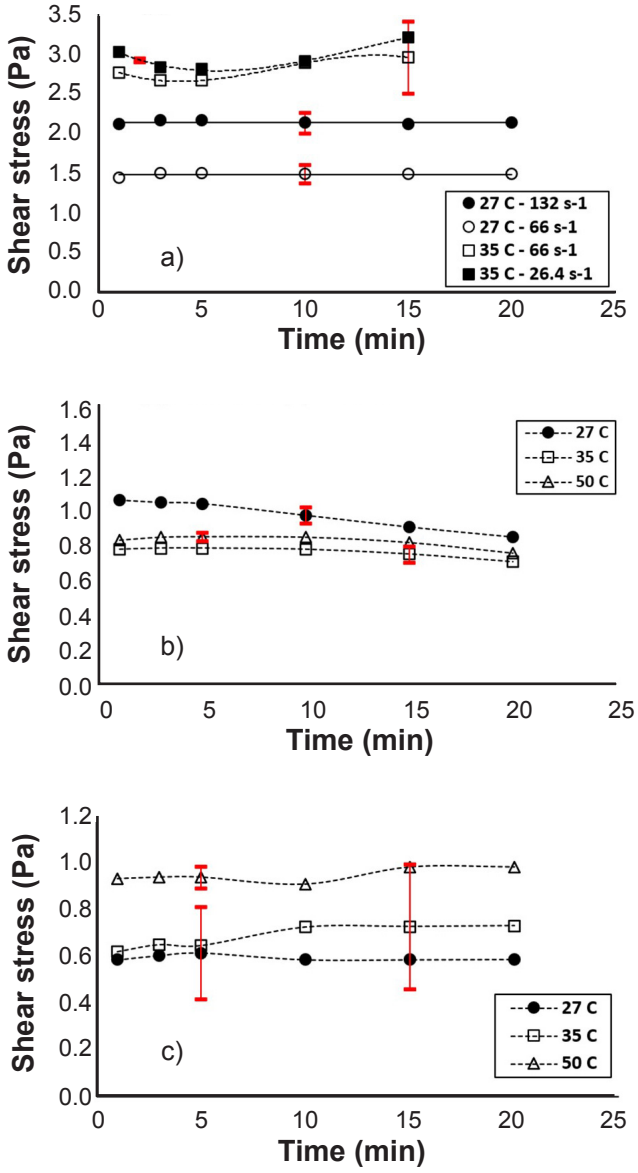

Figure 6: Shear stress as a function of time at constant shear rate and temperature: a) HM-B32 pulp; b) HM-B32-1 pulp at $\dot{\gamma}$=66 s^{-1}; and c) HM-B32-3 pulp at $\dot{\gamma}$=66 s^{-1} (lines link data without any statistical treatment).

time for both $\dot{\gamma}$ used, as a thixotropic fluid. Fig. 6b presents a typical τ vs. t data for this pulp. Increasing the dispersant concentration from 1% to 2-3%, τ tended to increase slightly with time after 5 min of the experiment at T>27 °C (Fig. 6c). Moreover, there was an inversion in τ vs. t curves as the temperature rose, i.e., τ values at 27 °C were lower than those at 35 and 50 °C. At 35 °C, considerable oscillations were detected in τ values enhancing the experimental error as seen in Fig. 6c. Such transitional rheological behaviors observed for both $\dot{\gamma}$ used (66 and 132 s^{-1}) may relate to additional particles-clusters interactions. Note that hydrocluster formation occurs even with dispersant because it depends on hydrodynamic forces developed during the shear flow [25]. Depending on dispersant properties and its concentration on the particle surface, as well as, the type of molecules or ions

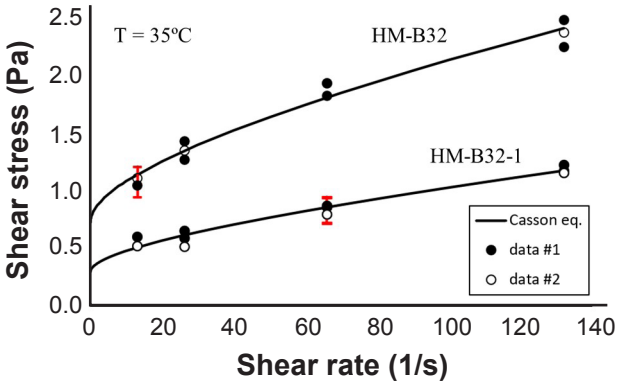

Figure 7: Typical shear stress as a function of shear rate curves at a constant temperature of 35 °C, for HM-B32 and HM-B32-1 pulps (data #1: τ vs. $\dot{\gamma}$ average values for the two first cycles; data #2: τ vs. $\dot{\gamma}$ average values for the last cycle; full line curves: best fitting of Casson model to data.

dispersed in the pulp, additional bridging interactions can appear between these constituents, hindering the particle-cluster mobility [24]. Since these interactions are weaker, they can be formed and broken quickly, giving greater oscillation, complexity, and instability in the pulp flow.

Typical τ vs. $\dot{\gamma}$ curve for HM-B32 and HM-B32-1 pulps are presented in Fig. 7. Experimental data obtained in all three cycles (descending τ-$\dot{\gamma}$ ramp; ascending τ-$\dot{\gamma}$ ramp; pulp rest/descending τ-$\dot{\gamma}$ ramp) did not differ from each other following the statistical analysis based on the experimental replication error, meaning that the hysteresis loop in τ vs. $\dot{\gamma}$ curve was statically insignificant for these two pulps. Based on the statistical analysis, the Casson model (Eq. B) fitted well these τ vs. $\dot{\gamma}$ data for the three temperatures analyzed. Data from Fig. 7 at 35 °C presented a typical fitting behavior for these two pulps. In Eq. B, τ_{0C} is the critical shear stress required for shearing the material and η_C is the apparent fluid viscosity, following the Casson model (subscript C). Both variables are the Casson model parameters, determined by fitting Eq. B to τ vs. $\dot{\gamma}$ data. Values of τ_{0C} are related to particle-cluster interactions (solid-like characteristics of the pulp) and η_C the viscous flow behavior (liquid-like characteristics of the pulp). For HM-B32 pulp, τ_{0C} and η_C varied from 0.43 to 1.81 Pa and from 4.9 to 2.1 mPa.s, respectively, as the temperature rose from 27 to 50 °C; on the other hand, for HM-B32-1 pulp, τ_{0C} and η_C varied from 0.37 to 0.45 Pa and from 2.5 to 1.1 mPa.s, respectively, as the temperature rose from 27 to 50 °C. A comparison between τ_{0C} values for HM-B32 and HM-B32-1 corroborated that the addition of X_{disp}=1% contributed to reducing: i) τ_{0C}, mainly at T>27 °C, improving the pulp condition to start flowing; and ii) η_C, improving the pulp condition to flow and implying a low apparent viscosity at high $\dot{\gamma}$. It is important to stress that the HM-B32 and HM-B32-1 pulp rheological behavior depended on time. Therefore, τ_{0C} and η_C values presented were restricted to a small-time interval of t=3 h after their production in the reactor mill equipment. Because of the instabilities in the shear flow for HM-B32-2 and HM-B32-3

pulps due to the additional particle-cluster interactions, τ vs. $\dot{\gamma}$ data depended also on the previous pulp shearing history (τ vs. $\dot{\gamma}$ curves in cycles 1, 2, and 3 differed from each one). These two pulps were considered unstable and eliminated from this analysis.

$$\tau^{1/2}=\tau_{0C}^{1/2}+(\eta_C.\dot{\gamma})^{1/2} \quad (B)$$

Reactive HM-A30 pulps: the τ vs. t and τ vs. $\dot{\gamma}$ data obtained for HM-A30 pulps without and with NaPA dispersant showed a remarkable dependency on the previous pulp shearing history with great oscillations in τ values at higher values of $\dot{\gamma}$ and temperature T. As confirmed by sedimentation experiments, HM-A30 was the most heterogeneous pulp, behaving as flocculated suspensions. The elevated pulp heterogeneity (different particle-flake mobilities) associated with high $\dot{\gamma}$ (high centrifugal force) and T (low liquid phase viscosity) enabled particle migration to the rotating rotor wall. This generated a liquid lubricant layer with low solid concentrations on this rotating wall, induced by particles sliding on this wall. Such behavior caused disturbances in the pulp flow, oscillations, and negative deviations from the actual τ value. The τ vs. $\dot{\gamma}$ data for these HM-A30 pulps, mainly at 50 °C, resembled those data from the characteristic rheogram of flocculated suspensions that have this particle sliding behavior [26]. Heterogeneity, oscillations, and instability detected in the shear flow of the reactive HM-A30 pulps must prevent their further operation in the spray dryer. Therefore, these pulps must be conditioned with different additive agents to improve their homogeneity and fluidity, avoiding any flocculation disturbances in the flow regime.

Non-reactive HM-R pulps: five HM-R pulps were analyzed regarding their shear flow behavior: HM-R20, HM-R20-04, HM-R20-08, HM-R30-1, and HM-R30-2. For HM-R30 pulp no data were obtained even at 50 °C because of its high flow resistance that exceeded the device reading scale, corroborating its low particle mobility identified in sedimentation experiments. The τ vs. t data for these pulps were characterized by decreasing τ along the time, except at higher T and $\dot{\gamma}$ in which τ oscillated about a constant value. The τ vs. $\dot{\gamma}$ data adjusted well to the Casson model (Eq. B), except data obtained at 50 °C that oscillated from one to another replication increasing the experimental error. These τ vs. $\dot{\gamma}$ data at 50 °C seemed to depend on the previous pulp shearing history (τ vs. $\dot{\gamma}$ in cycles 1, 2, and 3 differed slightly from each one); however, such differences among data were in the range of experimental error. Therefore, the adjustment of these τ vs. $\dot{\gamma}$ data at 50 °C to Eq. B provided average values of the Casson model parameters within a high experimental error. Based on τ_{0C} and η_C values obtained by the fitting analysis, the following trends could be drawn for the HM-R pulps: i) a significant reduction in τ_{0C} occurred with the dispersant addition, improving the necessary condition for starting flow (similar to a trend observed for HM-B30 pulps); ii) for HM-R30-1 pulp, τ_{0C} and η_C reached values of 0.75, 1.09, and 0.70 Pa and 2.6, 0.7, and 1.7 mPa.s, respectively, as the temperature rose from 27 to 50 °C; and iii) an increase in X_{disp} from 1% to 2% in the HM-R30 pulps resulted in increasing τ_{0C} and reducing η_C. This meant that the HM-R30-2 pulp presented a great resistance to start flowing but, after overcoming τ_{0C}, this pulp flowed more easily. Such behavior implied a change of particle-cluster interactions at X_{disp}=2% in a way to restrain their mobility at the flow startup, corroborating the earlier discussion about the rheological behavior of HM-B32-2 and HM-B32-3 pulps. In the range of the operation conditions analyzed, a comparative analysis between the rheological behavior of HM-R30-1 and HM-B32-1 pulps confirmed the lowest τ_{0C} and η_C values for HM-B32-1 pulp during a short operating time (t≤3 h) and the most stable flow behavior for this pulp based on the replication τ vs. $\dot{\gamma}$ experimental data.

Preliminary experiments developed confirmed the feasibility of drying HM pulps in the spray dryer under specific operating conditions. However, to make the spray drying stage viable concerning the proposed process route, HM-powder must be produced continuously, without interruption due to the atomizer clogging. For that, the pulp must be fed in the spray dryer in an intermittent mode under rigid temperature control [27].

CONCLUSIONS

Two concentrated and reactive magnesium hydroxide (HM), $Mg(OH)_2$, pulps, HM-A (more impure) and HM-B (purer), were produced by caustic magnesia hydration in a reactor mill equipment, and they were characterized chemically and physically to evaluate the feasibility of drying them in a spray dryer. As discussed, the dispersant addition to these HM-concentrated pulps should be carefully analyzed since there was a restricted range of NaPA concentration at which this dispersant could improve the pulp flow. For non-reactive HM-R pulps, the fluid flow analysis confirmed the formation of hydroclusters. Their behavior aided in better understanding the reactive HM pulp fluid flow behavior since X_{HM} (HM mass/solid mass) was maintained constant during each experiment and its value could be easily varied from a diluted pulp to a concentrated one. As HM-A pulp became more concentrated, hydroclusters were also formed, hindering its flow. However, the heterogeneity of the HM-A pulp was the predominant restriction for operating it in the spray dryer. This HM-A pulp presented high impurities in its composition, resulting in the lowest X_{HM} value (from 78% to 82%). Reactive HM-pulps with high impurities (X_{HM}<90%) must be conditioned with different additive agents to improve their homogeneity and fluidity, before testing these pulps in the spray dryer stage. Although comparable to the one of a synthetic and non-reactive HM-pulp at ambient temperature, the flow behavior of HM-A and HM-B changed as the temperature increased due to the progress of the MgO hydration reaction. Both the water reaction consumption and the increase in HM contributed to concentrating more HM-B pulp. Considering all the above, this study allowed defining that, among all HM-pulps studied, HM-B32 pulp (HM-B with 32% solids) with 1% NaPA dispersant (HM-B32-1)

was the most stable one for a short processing period and presented the best flow behavior making this pulp the most suitable to be tested in a pilot spray dryer.

ACKNOWLEDGMENTS

The authors are immensely and sincerely grateful to Professor Maria Laura Passos for her precious contributions to this work. The authors are also grateful to the National Council for Scientific and Technological Development (CNPq) and the Research Support Foundation of the Minas Gerais State (FAPEMIG) for financial support.

REFERENCES

[1] K. Tong, X. Song, S. Sun, Y. Xu, J. Yu, Colloids Surf. A Physicochem. Eng. Asp. **436** (2013) 1111.
[2] Q. Wu, P.L. Bishop, T.C. Keener, J. Stallard, L. Stile, Water Sci. Technol. **44**, 1 (2001) 161.
[3] A. Pilarska, K. Bula, K. Myszka, T. Rozmanowski, K. Szwarc-Rzepka, K. Pilarski, Ł. Chrzanowski, K. Czaczyk, T. Jesionowski, Open Chem. **13**, 1 (2015) 161.
[4] S.D.F. Rocha, V.S.T. Ciminelli, Polímeros **11**, 3 (2001) 116.
[5] H.N. Costa, C.C. Noberto, L.A. Almeida, R.E.F.Q. Nogueira, A.E.B. Cabral, Cerâmica **67**, 384 (2021) 399.
[6] A. Thakore, J.O.B. Ringrose, A. Gibson, M. Wajer, Pulp Pap. Canada **106**, 5 (2005) 46.
[7] J.H.M. Viana, A.M. Coelho, A. Thomazini, M.P.F. Carvalho, An. Acad. Bras. Cien. **93**, 3 (2021) e20201614.
[8] A.A. Pilarska, Ł. Klapiszewski, T. Jesionowski, Powder Technol. **319** (2017) 373.
[9] A. Pilarska, E. Markiewicz, F. Ciesielczyk, T. Jesionowski, Dry. Technol. **29**, 10 (2011) 1210.
[10] U.S. Geological Survey, "Mineral commodity summaries" (2022).
[11] S.D.F. Rocha, M.B. Mansur, V.S.T. Ciminelli, J. Chem. Technol. Biotechnol. **79**, 8 (2004) 816.
[12] V.S. Birchal, S.D.F. Rocha, M.B. Mansur, V.S.T., Ciminelli, Can. J. Chem. Eng. **79**, 4 (2001) 507.
[13] D.M. Núñez Ramírez, L. Medina-Torres, F. Calderas, R.H. Lara RH, H. Medrano Roldán, O. Manero, Miner. Eng. **121** (2018) 122.
[14] H. Aral, M.R. Houchin, P.R. Strode, R. Van Merkestein, P. Bush, US Patent 5906804A (1999).
[15] H. Sano, N. Matsuno, K. Okina, US Patent 3957674A (1976).
[16] S. Mueller, E.W. Llewellin, H.M. Mader, Proc. R. Soc. London A **466**, 2116 (2010) 1201.
[17] J.Z.Q. Zhou, T. Fang, G. Luo, P.H.T. Uhlherr, Rheol. Acta **34** (1995) 544.
[18] C.M.F. Santos, A.F.B. Andrade, K.C. Ferreira, S.D.F. Rocha, Braz. Appl. Sci. Rev. **3**, 4 (2019) 1882.
[19] R.J. Falcione, R.R. McManis, J.A. Aufman, US Patent 4230610A (1980).
[20] A.P.G. Lockwood, J. Peakall, N.J. Warren, G. Randall, M. Barnes, D. Harbottle, T.N. Hunter, Chem. Eng. Sci. **231** (2021) 116274
[21] B.A. Di Giovanni, F.M. Mahdi, V.M. Starov, R.G. Holdich, Chem. Eng. Res. Des. **90**, 9 (2012) 1168.
[22] G. Balducci, L.B. Diaz, D.H. Gregory, CrystEngComm **19**, 41 (2017) 6067.
[23] B. Camenen, D.P. Van Bang, Cont. Shelf Res. **31**, 10 (2011) 106.
[24] F.S. Ortega, V.C. Pandolfelli, J.A. Rodrígues, P.A. Sepúlveda, Cerâm. Ind. **2**, 5-6 (1997) 34.
[25] J. Warren, S. Offenberg, H. Toghiani, C.U. Pittman Jr., T.E. Lacy, S. Kundu, ACS Appl. Mater. Interfaces **7**, 33 (2015) 18650.
[26] N.G. Triantafillopoulos, *Measurement of fluid rheology and interpretation of rheograms*, Kaltec Scient., Livonia (1988) 37.
[27] M.L. Passos, A.L.G. Trindade, J.V.H. D'Angelo, M. Cardoso, Dry. Technol. **22**, 5 (2004) 1041.
(Rec. 04/11/2022, Ac. 07/12/2022)